Inorganic Chemistry

Article

pubs.acs.org/IC

Search for Electron Delocalization from $[Fe(CN)_6]^{3-}$ to the Dication of Viologen in $(DNP)_3[Fe(CN)_6]_2 \cdot 10H_2O$

Ahmed S. Abouelwafa,[*,†,‡,¶] Andreas Hauser,[†] Valeriu Mereacre,[‡] Yanhua Lan,[‡] Gary J. Long,[*,§] Fernande Grandjean,[§,∥] Gernot Buth,[⊥] Christopher E. Anson,[‡] and Annie K. Powell[*,‡,#]

[†]Département de Chimie Physique, Université de Genève, 30 Quai Ernest Ansermet, CH-1211 Genève, Switzerland

[‡]Institut für Anorganische Chemie, Karlsruhe Institute of Technology, Engesserstrasse 15, D-76131 Karlsruhe, Germany

[§]Department of Chemistry, Missouri University of Science and Technology, University of Missouri, Rolla, Missouri 65409-0010, United States

[∥]Faculty of Sciences, University of Liège, B-4000 Sart-Tilman, Belgium

[⊥]Institut für Beschleunigerphysik und Technologie and [#]Institut für Nanotechnologie, Karlsruhe Institute of Technology, Hermann-von-Helmholtz-Platz 1, D-76344 Eggenstein-Leopoldshafen, Germany

Supporting Information

ABSTRACT: $K_3Fe(CN)_6$ reacts with the viologen 1,1′-bis(2,4-dinitrophenyl)-4,4′-bipyridinium dication, $(DNP)^{2+}$, to form a supramolecular complex, $(DNP)_3[Fe(CN)_6]_2 \cdot 10H_2O$ (**1**). The crystal structure of **1** reveals that there are two $[Fe(CN)_6]^{3-}$ anions within an organic framework of three $(DNP)^{2+}$ cations with the shortest Fe(III)···Fe(III) distances of ca. 9.8 Å, distances that minimize extensive long-range magnetic exchange coupling interactions between the $[Fe(CN)_6]^{3-}$ anions, and, thus, **1** is paramagnetic above ca. 17 K and exhibits weak ferromagnetic coupling between 17 and 3 K and antiferromagnetic coupling between 3 and 1.8 K. The long Fe(III)···Fe(III) distances permit slow spin−spin and slow spin−lattice paramagnetic relaxation, relative to the iron-57 Larmor precession frequency, as is evidenced by the Mössbauer spectra measured between 3 and 60 K; between 85 and 295 K, rapid paramagnetic relaxation is observed. Both the slow spin−spin and slow spin−lattice relaxation are mediated by the organic, π-conjugated viologen cations. The Fe−C distances, the Mössbauer isomer shifts, the temperature dependence of the magnetic susceptibility, and the 3 K magnetization results all indicate the presence of low-spin Fe(III) ions in the $[Fe(CN)_6]^{3-}$ anions in **1**. There is no unequivocal indication of the presence of any formal electron delocalization or transfer from the $[Fe(CN)_6]^{3-}$ anion to the $(DNP)^{2+}$ cations in the results obtained from X-ray crystallography, magnetic measurements, and Mössbauer spectra. Because of enhancement of the spin−orbit coupling by the heavy-atom or -ion effect, the Fe(III) ions in the $[Fe(CN)_6]^{3-}$ anions interact with the $(DNP)^{2+}$ cations, causing them to fluoresce with increasing intensity upon cooling from 90 to 25 K when excited at 300 nm. The resulting luminescence of the viologen $(DNP)^{2+}$ cation induced by the $[Fe(CN)_6]^{3-}$ anions indicates the presence of significant mixing of the molecular orbitals derived from the $[Fe(CN)_6]^{3-}$ anions and the molecular orbitals associated with the $(DNP)^{2+}$ cations to yield bonding supramolecular orbitals in **1**, a mixing that is also observed between 50 and 3 K in the temperature dependence of the isomer shift of **1**.

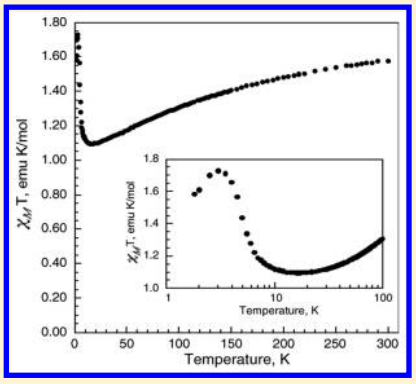

INTRODUCTION

Inorganic chemistry is enriched by different structural motifs[1] that display interesting magnetic properties, such as isolated molecules that display the slow relaxation of their magnetization, i.e., single-molecule magnets or one- and two-dimensional chain polymers.[2] The magnetic interactions in these compounds are usually mediated by bridging ligands, such as oxide, hydroxide, alcholates, azides, nitriles, or oxalate anions, resulting in superexchange between different paramagnetic metal ions.[2,3] However, the chemistry of structurally characterized salts containing cations and anions that display slow paramagnetic relaxation is relatively underdeveloped in low-spin iron(III) complexes. This probably results because of the challenge of "dispersing" low-spin Fe(III) ions in structurally characterized lattices, in which the shortest Fe(III)···Fe(III) distance is greater than ca. 7 Å, a separation that would typically permit long spin−spin relaxation times[4] in order to yield slow paramagnetic relaxation of the low-spin, $S = {}^1/_2$, Fe(III).

There have been some reports dealing with high-spin Fe(III) ions displaying slow paramagnetic relaxation, such as the iron(III) chloride α-diamine complex,[5] a variety of tetrachloroferrate analogues,[6] and iron(III) compounds containing dithiochelates.[7] The majority of the iron(III) dithiocarbamate complexes exhibit intermediate values of their room-temperature magnetic moments, values between the high-spin, $S = {}^5/_2$, and

Received: March 1, 2017
Published: May 16, 2017

© 2017 American Chemical Society

DOI: 10.1021/acs.inorgchem.7b00540
Inorg. Chem. 2017, 56, 6477−6488

low-spin, $S = {}^1/_2$, states resulting from "a thermal equilibrium between the two spin-states."[7b,e,8] The only exceptions are the diisopropyl-, diisobutyl-, and dicyclohexylcarbamate derivatives, which are found, at all temperatures, to contain exclusively the low-spin Fe(III) electronic state based on their Mössbauer spectral[7b,9] and magnetic properties.[8] The model developed by Wignall,[4] which indicates that a minimum metal cation−metal cation distance of ca. 7 Å is an important criterion for observing slow paramagnetic relaxation, is valid in all of the above-mentioned examples.

Some of the present authors have recently published a report[10] on the photoenhanced and thermally enhanced electron transfer from a $[Fe(CN)_6]^{4-}$ anion to the viologen dication electron acceptor, 1,1′-bis(2,4-dinitrophenyl)-4,4′-bipyridinium, $(DNP)^{2+}$.

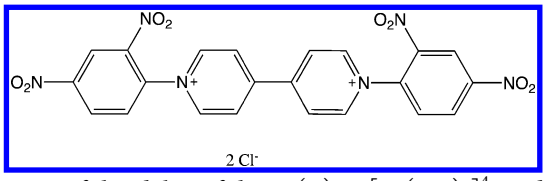

Because of the ability of the Fe(II) in $[Fe(CN)_6]^{4-}$ to be, at least in part, oxidized to Fe(III) to form $[Fe(CN)_6]^{3-}$, a spontaneous partial electron transfer from the $[Fe(CN)_6]^{4-}$ anion to the $(DNP)^{2+}$ acceptor occurs[10] and is further enhanced either by irradiating the complex with sunlight or 254 nm UV radiation or by heating to 95 °C. This observation has motivated our study of the interactions between $[Fe(CN)_6]^{3-}$, derived from the $K_3Fe(CN)_6$ starting reactant, with the electron-deficient 4,4′-bipyridinium core of the viologen dications, both to monitor electron transfer between the anion and cation and to form a structure in which the paramagnetic low-spin Fe(III), in the $[Fe(CN)_6]^{3-}$ anions, are sufficiently separated within a lattice of large organic groups to both limit direct dipolar exchange interactions and increase the temperature range over which the reduced spin−spin and spin−lattice coupling slows the rate of paramagnetic relaxation.

To achieve this goal, the room temperature reaction of 1,1′-bis(2,4-dinitrophenyl)-4,4′-bipyridinium dichloride, $(DNP)Cl_2$, with $K_3Fe(CN)_6$ was used to prepare $(DNP)_3[Fe(CN)_6]_2 \cdot 10H_2O$ (**1**), a supramolecular complex in which the shortest Fe(III)···Fe(III) distance between the $[Fe(CN)_6]^{3-}$ anions is ca. 9.8 Å. Wignall's concept therefore applies, and **1** displays both slow spin−spin relaxation below ca. 30 K and slow spin−lattice relaxation between ca. 30 and 77 K, as is indicated by both iron-57 Mössbauer and photoluminescence spectroscopy. Mössbauer spectral, magnetic susceptibility, and colorimetric measurements all reveal a low-spin Fe(III) ion in $[Fe(CN)_6]^{3-}$ with no formal electron transfer from $[Fe(CN)_6]^{3-}$ to the $(DNP)^{2+}$ dications in **1**.

EXPERIMENTAL SECTION

Synthesis. $(DNP)_3[Fe(CN)_6]_2 \cdot 10H_2O$ (**1**) has been synthesized through the addition of $K_3Fe(CN)_6$ (0.0108 g, 0.033 mmol) to a stirred solution of $(DNP)Cl_2$ (0.021 g, 0.033 mmol) in 50 mL of distilled water. The solution was stirred at ambient temperature for a further 20 h and then filtered. The resulting clear yellow solution was kept undisturbed at ambient temperature to yield, after 4 weeks, small yellow needle-shaped crystals and a microcrystalline powder. Yield: 75% (30% in crystalline form). Elem anal. Calcd for **1**, after the loss of one lattice water molecule, $C_{78}H_{60}Fe_2N_{30}O_{33}$: C, 45.54; H, 2.94; N, 20.43. Found: C, 45.62; H, 2.54; N, 20.24. The amounts of C, N, and H atoms were determined by using an Elementar Vario EL analyzer. ***Caution!*** *Viologens, with the registered trade name "Paraquat", are toxic herbicides and should be handled with caution. Also cyanide-containing compounds should be kept away from acids.*

Crystallography. Measurements were made at 150 K on the SCD beamline of the Synchrotron Light Source ANKA at the Karlsruhe Institute of Technology, by using a Bruker SMART Apex diffractometer with silicon-monochromated X-ray radiation with λ = 0.8000 Å. No significant diffraction intensity could be measured above a resolution of 0.88 Å. The reflection intensities have been corrected for absorption and primary beam decay using the *SADABS* code.[11a] The structure was solved by direct methods and refined by using the *SHELXL-2014* software package.[11b] All non-H atoms and ions were refined with anisotropic thermal parameters except for the minor disordered component of one of the lattice water molecules. Organic H atoms were placed in calculated positions by using a riding model; it was possible to locate and refine the H atoms of four of the lattice water molecules. Crystallographic data and details of the structure refinement are listed in Table 1. A crystallographic information file for **1** is available as CCDC 1476568.

Table 1. Crystal and Refinement Parameters for 1

molecular formula	$C_{78}H_{62}Fe_2N_{30}O_{34}$
fw, g/mol	2075.27
cryst syst	monoclinic
space group	$P2_1/c$
a, Å	21.2623(14)
b, Å	21.4806(15)
c, Å	19.3971(13)
β, deg	94.700(1)
V, Å^3	8829.4(10)
Z	4
T, K	150(2)
F(000)	4256
D_c, g/cm^3	1.561
λ, Å	0.8000
μ (0.8 Å), mm^{-1}	0.575
reflns measd	27166
unique reflns	13307
R_{int}	0.0265
data with $I \geq 2\sigma(I)$	11195
wR2 (all data)	0.1463
S (all data)	1.029
R1 [$I \geq 2\sigma(I)$]	0.0512
no. of param/restraints	1325/12
largest diff peak/hole, e/Å^3	+0.95/−0.71

Magnetic Measurements. Magnetic susceptibility measurements have been obtained by using a Quantum Design MPMS-XL SQUID magnetometer. The direct-current molar magnetic susceptibility of a polycrystalline sample of **1**, sealed and anchored in a polyethylene bag, was measured at 0.1 T upon field cooling from 300 to 1.8 K. The magnetization was then subsequently and immediately measured at 1.8 K in a 0−7 T applied magnetic field. The resulting molar magnetic susceptibility was corrected for the contribution of the polyethylene bag and for the intrinsic core diamagnetic contribution of −0.000970 emu/mol, a value obtained from Pascal's constants.[12]

Mössbauer Spectroscopy. The iron-57 Mössbauer spectra of **1** have been measured between 3 and 295 K in zero applied field, at 3 K in transverse applied fields of 3, 4, 5, and 6.5 T, and at 77, 150, and 295 K in a transverse applied field of 6.5 T, on two different constant-acceleration spectrometers that utilized room temperature cobalt-57 sources in a rhodium matrix and were calibrated at 295 K with α-iron. The absorber thickness was ca. 50 mg/cm^2 of **1**. The isomer shifts are referred to α-iron at 295 K. The observed spectra have been fitted as discussed below.

Photoluminescence Spectroscopy. Solid-state emission and excitation spectra were collected by using a Photon Technology International QuantaMaster-1046 model spectrophotometer and a Janis

DOI: 10.1021/acs.inorgchem.7b00540
Inorg. Chem. 2017, 56, 6477−6488

Table 2. Bond Lengths for the $[Fe(CN)_6]^{3-}$ Anions in 1

Fe−C distance, Å	Fe(1)−C(1)	1.952(4)	Fe(2)−C(7)	1.935(4)
	Fe(1)−C(2)	1.940(3)	Fe(2)−C(8)	1.936(4)
	Fe(1)−C(3)	1.946(4)	Fe(2)−C(9)	1.936(3)
	Fe(1)−C(4)	1.939(4)	Fe(2)−C(10)	1.944(4)
	Fe(1)−C(5)	1.935(3)	Fe(2)−C(11)	1.926(4)
	Fe(1)−C(6)	1.930(3)	Fe(2)−C(12)	1.942(4)
average Fe−C distance, Å	Fe(1)	1.941(4)	Fe(2)	1.937(4)
average C−N distance, Å	Fe(1)	1.147(2)	Fe(2)	1.148(2)
Fe−C bond distance distortion, %	Fe(1)	0.29	Fe(2)	0.28
C−Fe−C bond angle distortion, %	Fe(1)	2.48	Fe(2)	4.86

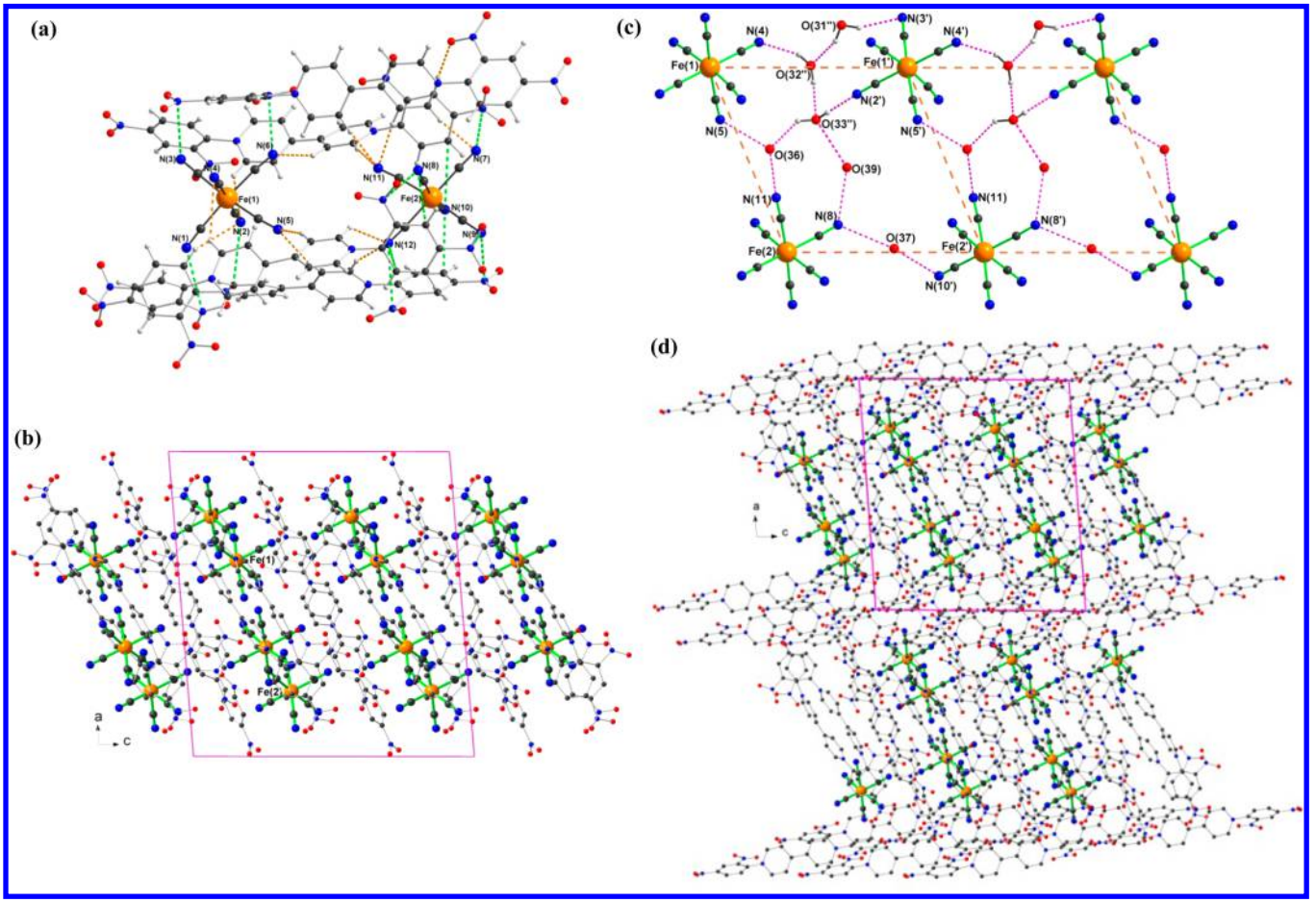

Figure 1. Supramolecular structure of **1**. (a) Interactions of the $[Fe(CN)_6]^{3-}$ anions with four surrounding $(DNP)^{2+}$ cations. The CN···N and CN···C π interactions are shown as green dotted lines, and the CN···HC hydrogen bonds are shown as orange dotted lines. (b) Layer of $[Fe(CN)_6]^{3-}$ anions interacting through both Fe(1) and Fe(2) with two of the layered $(DNP)^{2+}$ cations. (c) $[Fe(CN)_6]^{3-}$ ladder structure parallel to the *c* axis, with the Fe(III)···Fe(III) distances that are under 10 Å shown as orange dashed lines. The hydrogen bonds are shown as purple dotted lines. (d) Intercalation of the $[Fe(CN)_6]^{3-}$ and $(DNP)^{2+}$ layers shown in part b by layers of the third $(DNP)^{2+}$ cation, which lies approximately perpendicular to the other two $(DNP)^{2+}$ dications.

ST-100 optical cryostat to record emission and excitation spectra at low temperatures. The temperature-dependent emission and excitation spectra were recorded with a Horiba Fluorolog 3 luminescence spectrometer with the sample inside a closed-cycle Oxford Instruments CCC1204 cryostat. For excitation at 300 nm, the third harmonic of a Quantel Brilliant B pulsed Nd:YAG laser was used; the overall time resolution of the system was 10 ns.

IR Spectroscopy. The Fourier transform IR spectra were measured on a PerkinElmer Spectrum One spectrometer between 400 and 4000 cm^{-1} in transmission mode by using eight scans that yield a resolution of 4 cm^{-1}. The absorbers were prepared by mixing both $(DNP)Cl_2$ and **1** with KBr in an ca. 1:30 ratio. A 1-cm-diameter disk of the sample was obtained by applying 10 tons or a force of ca. 98000 N under vacuum.

Electron Paramagnetic Resonance (EPR) Spectroscopy. Standard X-band EPR measurements of a powder sample of **1** were measured at 4 K with a Bruker ESP300E spectrometer equipped with an Oxford Instruments cryostat. The spectral results of this work are presented in the Supporting Information.

RESULTS AND DISCUSSION

Crystal Structure. In an aqueous solution, 3 mol of the viologen, $(DNP)Cl_2$, react immediately with 2 mol of $K_3Fe(CN)_6$ to form an intense yellow solution, which after precipitation and recrystallization leads to small, weakly diffracting, yellow crystals suitable for a successful character-

DOI: 10.1021/acs.inorgchem.7b00540
Inorg. Chem. 2017, 56, 6477−6488

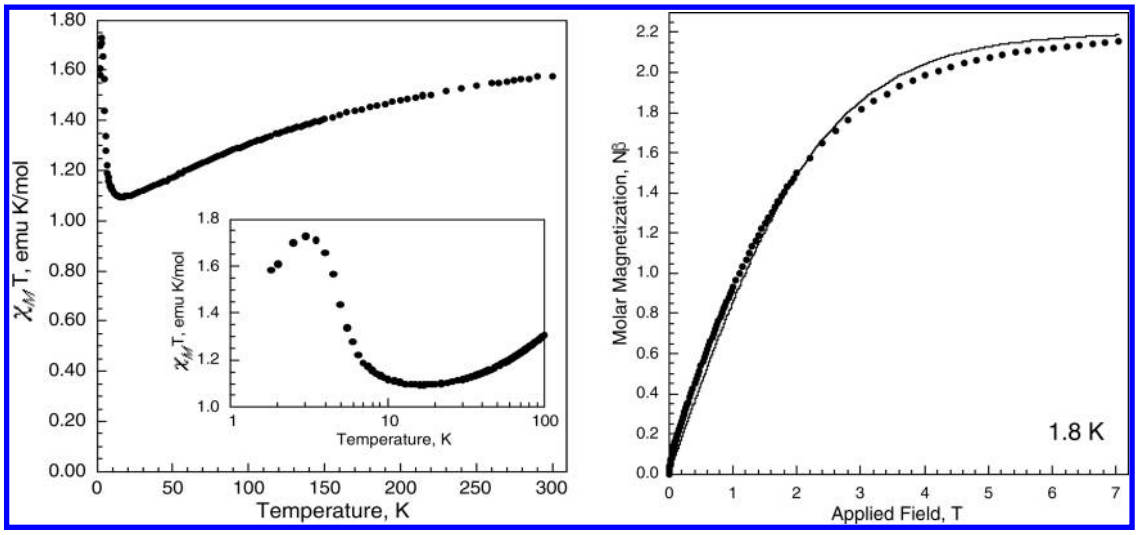

Figure 2. Left: Temperature dependence of $\chi_M T$ for **1** measured at 0.1 T upon field cooling from 300 to 1.8 K. Inset: Semilogarithm plot of the temperature dependence of $\chi_M T$ between 1.8 and 100 K. Right: 1.8 K magnetization of **1** obtained between 0 and 7 T. The solid line corresponds to a Brillouin fit calculated for the two low-spin Fe(III) ions in **1** each with $S = {}^1/_2$ and with an average g value of 2.22(1).

ization by X-ray crystallography with a synchrotron radiation source. The absence of a green or blue color indicates little if any formal electron transfer from the $[Fe(CN)_6]^{3-}$ anions to the $(DNP)^{2+}$ cations in **1**. X-ray characterization has revealed a supramolecular complex with the stoichiometry, $(DNP)_3[Fe(CN)_6]2{\cdot}10H_2O$, **1**. Compound **1** crystallizes in the monoclinic $P2_1/c$ space group, with three viologen dications, two $[Fe(CN)_6]^{3-}$ anions, and 10 noncoordinated water molecules in the asymmetric unit. At 150 K, the Fe−C distances in the $[Fe(CN)_6]^{3-}$ anions are in the range of 1.926(4)−1.952(4) Å, with average Fe(1)−C and Fe(2)−C values of 1.939(4) Å. The 150 K Fe−C bond lengths are thus in good agreement with the Fe−C distances of 1.941 Å at 295 K and 1.943(1) Å at 100 K found[13] in $K_3Fe(CN)_6$. The shortest 150 K Fe(III)···Fe(III) distances are 9.793 Å from Fe(2) to its symmetry equivalent Fe(2), 9.818 Å from Fe(1) to its symmetry equivalent Fe(1), and 9.828 Å from Fe(1) to Fe(2); all other such distances are larger than 10.9 Å.

The structures of the two crystallographically distinct $[Fe(CN)_6]^{3-}$ anions in **1** are rather similar (see Table 2 and Figure 1a), but there are small differences in their coordination environments. The Fe(1) site exhibits a highly distorted pseudooctahedral or close to C_3 symmetry environment in which the three C(1)−Fe(1)−C(6), C(2)−Fe(1)−C(4), and C(3)−Fe(1)−C(5) distances of 3.882(7), 3.879(7), and 3.881(7) Å, respectively, are not significantly different. In contrast, the Fe(2) site exhibits a slightly tetragonally compressed pseudooctahedral or close to C_2 symmetry environment in which the axial C(9)−Fe(2)−C(11) distance of 3.862(7) Å is at best slightly shorter than the two essentially equivalent, within their uncertainties, equatorial C(7)−Fe(2)−C(12) and C(8)−Fe(2)−C(10) distances of 3.877(8) and 3.880(8) Å, respectively. As will be seen below, these small distance differences in conjunction with the associated different coordination angles are sufficient to yield different hyperfine parameters for Fe(1) and Fe(2) between 85 and 295 K.

The two $[Fe(CN)_6]^{3-}$ anions in **1** interact, primarily through the cyanide nitrogen lone pairs, with four surrounding viologen dications, 1 and 2, and their symmetry equivalents (see Figure 1a). The interactions can be categorized as (i) to nitrogen atoms of the nitro groups with a shortest CN···N distance of 2.916 Å, (ii) to the p electrons on aromatic carbons, with a shortest CN···C distance of 3.011 Å, and (iii) CN···HC hydrogen bonds with a shortest CN···C distance of 3.131 Å. These rather strong supramolecular interactions yield layers composed of $[Fe(CN)_6]^{3-}$ and $(DNP)^{2+}$ ions, which run parallel to the (100) crystal plane, a plane in which the $(DNP)^{2+}$ cations are roughly parallel (see Figure 1b). Within these layers, the closest Fe(III)···Fe(III) separations are between $[Fe(CN)_6]^{3-}$ anions that are arranged in distorted ladder-like arrays. In Figure 1c, the Fe(III)···Fe(III) distances under 10 Å, i.e., 9.793, 9.818, and 9.828 Å, are indicated by orange dotted lines. In addition to interactions with the $(DNP)^{2+}$ cations, these arrays are stabilized by hydrogen bonding involving some of the lattice water molecules. In particular, O(36) and O(37) each make hydrogen bonds to cyanide nitrogen atoms from different $[Fe(CN)_6]^{3-}$ anions, thus acting as direct linkages, although the O···N distances are quite long at 3.061−3.156 Å.

The third viologen $(DNP)^{2+}$ cation in the asymmetric unit does not interact directly with the $[Fe(CN)_6]^{3-}$ anions but does interact with the other $(DNP)^{2+}$ cations, principally through a combination of CH···ON hydrogen bonds and intermolecular electrostatic interactions between an oxygen atom of one nitro group and the nitrogen atom of another group with a shortest such O···N distance of 3.011 Å. This third $(DNP)^{2+}$ cation lies with its long axis approximately perpendicular to those of the other two $(DNP)^{2+}$ cations and yields layers that alternate with the $[Fe(CN)_6]^{3-}$ and $(DNP)^{2+}$ layers described in the previous paragraph (see Figure 1d). The Fe−C bond lengths and average values for **1** are listed in Table 2.

Finally, the crystal structure of **1** is essentially a compact structure with an extensive number of bonding pathways between the $[Fe(CN)_6]^{3-}$ anions and the $(DNP)^{2+}$ cations that are shorter than the sum of the covalent van der Waals radii of the atoms or ions involved. The extensive number of these pathways facilitates an effective spin−lattice coupling of the low-spin Fe(III) cations in the $[Fe(CN)_6]^{3-}$ anions, with the phonon modes present in **1**, a coupling that exhibits a strong temperature dependence. The presence and extent of this coupling, along with spin−spin coupling, leads, as will be shown below, to the onset of slow paramagnetic relaxation of the low-spin, $S = {}^1/_2$, Fe(III) moments below ca. 50 K.

DOI: 10.1021/acs.inorgchem.7b00540
Inorg. Chem. 2017, 56, 6477−6488

Magnetic Measurements. The temperature dependence of the molar magnetic susceptibility, χ_M, of **1** has been measured at 0.1 T upon field cooling from 300 to 1.8 K; the resulting $\chi_M T$, obtained after diamagnetic correction of χ_M, is shown in the left portion of Figure 2. After reaching 1.8 K, the molar magnetization of **1** was immediately measured from 0 to 7 T.

A plot of $1/\chi_M$ revealed substantial curvature below ca. 150 K; however, a modified Curie–Weiss fit of χ_M between 10 and 300 K with the expression

$$\chi_M = \chi_0 + \frac{C}{T - \theta}$$

led to a small χ_0 of 0.00250 emu/mol, a Curie constant, C, of 1.027 emu·K/mol, and a Weiss temperature, θ, of 0.53 K, all values of which are consistent with the presence of low-spin Fe(III) ions at the two crystallographically distinct $[Fe(CN)_6]^{3-}$ anions found in **1**. This fit conveniently provides an estimate of χ_0, the second-order Zeeman contribution to χ_M, i.e., the temperature-independent contribution to the molar magnetic susceptibility that results from mixing between the ground and first excited states; the observed value is reasonable for two low-spin Fe(III) ions, but its exact value may be influenced by small uncertainties in the diamagnetic correction, the sample mass, and/or the molecular weight if the sample studied has lost some of its water of hydration. The resulting Curie constant of 1.027 emu·K/mol observed between 10 and 300 K is substantially higher than the corresponding spin-only $\chi_M T$ value of 2(0.375) = 0.750 emu·K/mol for the two Fe(III) ions in **1** when $S = {}^1/_2$ and $g = 2$. Thus, the larger than spin-only value of $\chi_M T$ for **1** indicates the presence of a substantial but reasonable orbital contribution to the moments of the low-spin Fe(III) ions in **1**. No clear significance should be given to the Weiss temperature of 0.53 K because the fit with the modified Curie–Weiss law is dominated by the high-temperature dependence of the magnetic susceptibility. The observed $\chi_M T$ values for **1** (see Figure 2) decrease from 1.577 emu·K/mol at 300 K to a minimum of 1.096 emu·K/mol at 17 K, increase to a maximum of 1.728 emu·K/mol at 3 K, and finally decrease to 1.583 emu·K/mol at 1.8 K.

In the pseudooctahedral coordination environment in **1**, the nominal t_{2g} orbital ground-state degeneracy of the Fe(III) ions, in octahedral symmetry, will be removed by the low-symmetry component of the crystal field to yield a d_{xy} orbital and essentially degenerate d_{xz} and d_{yz} orbitals if the symmetry is close to axial. The coordination environments of both the Fe(1) and Fe(2) crystallographic sites in **1** are highly distorted (see Table 2). As a consequence, the point group symmetry of the two sites may be considered as nominally having C_3 or even C_2 symmetry. In the latter case, the d_{xz} and d_{yz} orbitals, of *b* symmetry, may or may not be approximately degenerate; in contrast, the d_{xy} orbital of *a* symmetry may have a rather different energy. Analysis of the Mössbauer spectral quadrupole splittings, discussed below, is consistent with this C_2 symmetry and also indicates that the d_{xy} orbital is the ground-state orbital and the essentially degenerate d_{xz} and d_{yz} are the first excited-state orbitals for both the Fe(1) and Fe(2) crystallographic sites in **1**.

Even though magnetic measurements alone cannot exclude the reverse ordering of these nominal t_{2g} orbitals, Mössbauer spectroscopy supports the above ordering of the orbitals and yields a splitting between the d_{xy} orbital and the essentially degenerate d_{xz} and d_{yz} orbitals of 380 cm^{-1}. As a consequence, the unpaired electron in the essentially degenerate d_{xz} and d_{yz} excited-state orbitals with $S = {}^1/_2$ and $M_L = \pm 1$ may be expected to make an orbital contribution to $\chi_M T$, which can then be as large as 1.25 emu·K/mol in **1**. Thus, there may be either an orbital state mixing and/or a spin–orbit interaction that further increases $\chi_M T$ at higher temperatures to yield the observed value of 1.577 emu·K/mol at 300 K; the currently available observations cannot yield a clear distinction between these two possibilities. Thus, in **1** and also, as noted[14] below, in $K_3Fe(CN)_6$, there is a substantial orbital contribution to the magnetic properties, but the ordering of the nominal t_{2g} orbitals is different in the two very different compounds.

The molar magnetization of **1** has also been measured at 1.8 K from 0 to 7 T (see the right portion of Figure 2). The magnetization exhibits a gradual increase with increasing applied field and saturates at 2.15 Nβ under 7 T, a value that is fully consistent with the presence in **1** of two low-spin Fe(III) ions, each with $S = {}^1/_2$. Further, the 1.8 K magnetization agrees well with the expected Brillouin dependence of the magnetization calculated for the two Fe(III) ions, each with $S = {}^1/_2$ and an average g value of 2.22(1) (see the solid line in the right portion of Figure 2). The good agreement between the 1.8 K magnetization and the Brillouin curve indicates that the antiferromagnetic exchange observed at 1.8 K in the decrease in $\chi_M T$, see below, is very weak.

It is instructive to compare the magnetic properties of **1** with those of the low-spin Fe(III) ion in $K_3Fe(CN)_6$,[14] which have been measured between 4 and 300 K by Baker and Figgis,[14b] in an unspecified applied magnetic field, probably 0.8 T or less.[14c] The results of their study have been converted to the equivalent χ_M values (emu/mol) and the resulting $\chi_M T$ values (emu·K/mol) and are shown in Figure S1. It is immediately apparent, at least between 50 and 300 K, that the observed temperature dependence of $\chi_M T$ for **1**, with two low-spin Fe(III) ions per mole, and that of the doubled $\chi_M T$ values for $K_3Fe(CN)_6$ are quite similar, with the values for **1** being higher by 0.24 and 0.14 emu·K/mol at 50 and 300 K, respectively; below ca. 50 K and especially below 17 K, the difference is more substantial. One can thus conclude that, at least above ca. 17 K, the magnetic properties of **1** and $K_3Fe(CN)_6$ are similar. However, on the basis of the quadrupole splitting observed[15] for **1** and $K_3Fe(CN)_6$, see below, the ordering of the t_{2g} orbitals is different in the two compounds. Further, it is clear that **1** exhibits a somewhat larger orbital contribution to the observed $\chi_M T$ values, perhaps because of its different ordering of the nominal t_{2g} orbitals. Hence, magnetic susceptibility measurements indicate that **1** and $K_3Fe(CN)_6$ contain low-spin Fe(III) ions in $[Fe(CN)_6]^{3-}$, with local coordination environments different enough to yield different ordering of the nominal t_{2g} orbitals.

Below ca. 17 K, the magnetic properties of **1** and $K_3Fe(CN)_6$ diverge (see Figure S1). We speculate that, between 17 and 3 K, the very weak ferromagnetic interaction between the two low-spin Fe(III) ions in **1**, separated by ca. 9.8 Å, becomes dominant perhaps within a layer (see the increase in $\chi_M T$ shown in the inset to the left portion of Figure 2), a ferromagnetic interaction that is apparently dominated below 3 K by a very weak long-range antiferromagnetic exchange, probably between the different layers shown in Figure 1d (see the decrease in $\chi_M T$ also shown in the inset to the left portion of Figure 2). No such complex magnetic ordering is present in $K_3Fe(CN)_6$ above 4 K. This is not surprising because the crystal structure[13] of $K_3Fe(CN)_6$ consists of rather well-isolated linear chains of $[Fe(CN)_6]^{3-}$ ions interconnected by only K^+ cations, and, as a consequence, $K_3Fe(CN)_6$ orders antiferromagnetically[16] at the very low temperature of $T_N = 0.129$ K.

DOI: 10.1021/acs.inorgchem.7b00540
Inorg. Chem. 2017, 56, 6477–6488

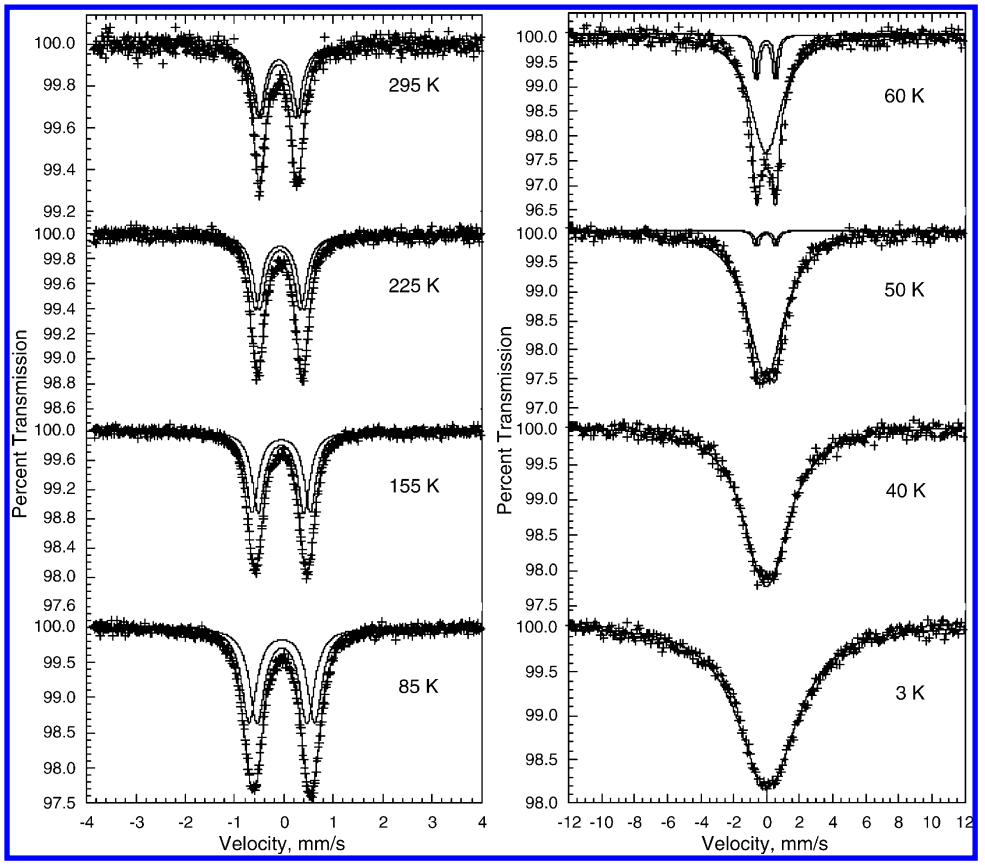

Figure 3. Left: Mössbauer spectra of **1** obtained at the indicated temperatures between 85 and 295 K and fit with two "nested" symmetric quadrupole doublets. Right: Spectra of **1** obtained at the indicated temperatures between 3 and 60 K and fit with an isotropic relaxation profile at 3 and 40 K and a combination of two quadrupole doublets and one relaxation profile at 50 and 60 K.

Mössbauer Spectroscopy. Although the mixed-valence iron(II)/iron(III) Prussian blue compounds are among the most extensively studied cyanide-containing compounds,[17] they typically contain low-spin Fe(II) bonded to six cyanide C atoms and high-spin Fe(III) bonded to six cyanide N atoms. In contrast, it must be noted that the low-spin Fe(III) in the two $[Fe(CN)_6]^{3-}$ anions in **1** and all of the low-spin Fe(III) ions in $K_3Fe(CN)_6$ are bonded to six cyanide C atoms, a difference that must be kept in mind in the evaluation of the Mössbauer spectral properties[15,17,18] of both compounds.

Iron-57 Mössbauer spectroscopy is an ideal technique[19] for characterizing the electronic structure, i.e., the oxidation and spin state of an Fe cation. It is typically easy to differentiate high-spin Fe(II) and high-spin Fe(III) by their isomer shifts, whereas it is more difficult to differentiate between low-spin Fe(II) and low-spin Fe(III). It is even more difficult to differentiate between low-spin Fe(III) with $S = {}^1/_2$ and low-spin Fe(IV) with $S = 1$, both of which exhibit isomer shifts relative to α-iron at 295 K of between −0.15 and +0.3 mm/s.[19] Nevertheless, in an attempt to either identify some Fe(IV) cations as a result of a formal electron transfer to the $(DNP)^{2+}$ cations or confirm the presence of two low-spin Fe(III) cations in **1**, its Mössbauer spectra have been measured from 3 to 295 K in a zero applied magnetic field; the higher-temperature spectra are shown in the left portion of Figure 3, and some of the lower-temperature spectra are shown in the right portion of Figure 3.

At and above 85 K, the Mössbauer spectra of **1** consist of two very similar quadrupole doublets, whereas between 40 and 3 K, the spectra consist of a broad featureless absorption that is characteristic of a slow isotropic paramagnetic relaxation. Between 85 and 40 K, the spectra consist of an admixture of both features. The parameters resulting from a fit of the spectra are given in Tables 3 and S1, and the temperature dependence of the spectral parameters is shown in Figure 4; the temperature dependence of the spectra is completely reversible. The spectra of **1** have also been measured in an applied field of up to 6.5 T at several temperatures (see below and the Supporting Information).

Table 3. Mössbauer Spectral Parameters of 1[a]

T, K	$\langle\delta\rangle$,[b] mm/s	ν, mm/s	ν,[c] MHz	area, %	spectral area, (% ε) mm/s
77	−0.037(2)	19.1(4)	223(5)	56(2)	7.98(6)
60	−0.036(7)	15.5(4)	180(5)	80(2)	8.8(1)
55	−0.032	13.4(3)	156(3)	94(1)	9.37(9)
50	−0.032	12.7(1)	147(1)	92(1)	9.25(4)
40	−0.02(1)	10.8(1)	125(1)	100	9.97(4)
30	−0.01(1)	9.5(1)	111(1)	100	
20	0.00(1)	8.1(1)	94(1)	100	10.8(1)
7	0.12(2)	7.9(2)	91(2)	100	
4.2	0.13(1)	8.2(2)	96(2)	100	
3	0.13(1)	8.2(1)	96(1)	100	11.0(1)

[a]The statistical uncertainties are given in parentheses; the actual uncertainties may be up to twice as large. The absence of an uncertainty indicates that the parameter was constrained to the value given. [b]The isomer shifts are given relative to 295 K α-iron. [c]The relaxing hyperfine field was fixed at 30 T, and the conversion factor was 11.6248 MHz/mm/s.

DOI: 10.1021/acs.inorgchem.7b00540
Inorg. Chem. 2017, 56, 6477−6488

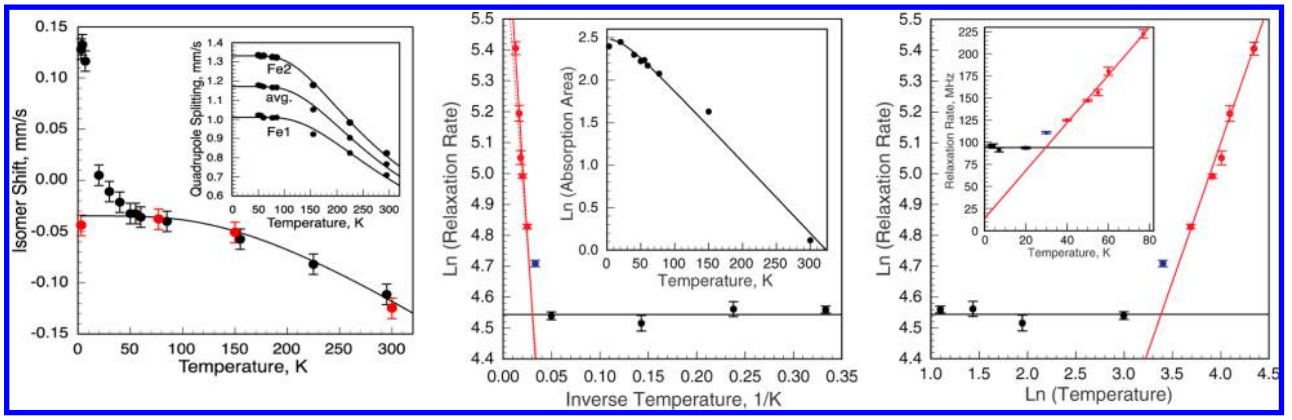

Figure 4. Left: Temperature dependence of the iron-57 Mössbauer effect average isomer shift of **1**. The black and red points are measured at 0 and 6.5 T applied field, respectively (see Table S2). The solid line is a fit with the Debye model for a solid between 50 and 295 K. Inset: Temperature dependence of the two quadrupole splittings of **1** and their average. The solid lines correspond to fits with the Ingalls model between 50 and 295 K. Center: Temperature dependence of the natural logarithm of the spectral absorption area of **1**, inset, and an Arrhenius plot of the relaxation rate. Right: Temperature dependence of the relaxation rate in **1**, inset, and the natural ln−ln plot of the temperature dependence of the relaxation rate.

Because the 150 K single-crystal structure of **1** reveals two crystallographically distinct Fe(1) and Fe(2) sites, its Mössbauer spectra obtained between 85 and 295 K have been fit with two symmetric equal area and line-width quadrupole doublets. These doublets have similar isomer shifts of −0.106(5) and −0.116(5) mm/s and somewhat different quadrupole splittings of 0.82(1) and 0.70(1) mm/s at 295 K. It should be noted that the alternative coupling of the absorption lines leads to somewhat different isomer shifts of −0.141 and −0.081 mm/s and similar quadrupole splittings of 0.75 and 0.77 mm/s. The former "nested" fit is preferred, and its parameters are given in Table S1 because this fit is most consistent with the structure of **1**, which reveals almost identical coordination environments with very similar average Fe−C bond distances of 1.941(4) and 1.937(4) Å, bond distance distortions of 0.29 and 0.28%, and bond angle distortions of 2.48 and 4.86% for the Fe(1) and Fe(2) sites, respectively. Thus, the "nested" site assignment given in Table S1 is based on the different percentage bond angle distortions. Furthermore, it is well established[20] that the isomer shift, δ, is more sensitive to the bond distance, whereas the quadrupole splitting, ΔE_Q, is more sensitive to both the bond distance and angle distortions. The alternate coupling of the four lines in the spectra between 77 and 295 K leads to two different isomer shifts, which are very different from those observed[15a] in $K_3Fe(CN)_6$. The spectra of **1**, obtained between 77 and 50 K, have been fit with a combination of one relaxation profile and two quadrupole doublets, the latter of which were, in part, constrained to have parameters that are consistent with those obtained at 85 K and above.

The temperature dependence of the average isomer shift is shown in Figure 4, left. The isomer shift values between 50 and 295 K are characteristic of either low-spin Fe(III) with $S = {}^1/_2$ or low-spin Fe(IV) with $S = 1$.[19] On the basis of the analysis of the magnetic susceptibility measurements (see above), the assignment to low-spin Fe(III) with $S = {}^1/_2$ is by far the most acceptable. Between 50 and 295 K, the uniform temperature dependence of the average isomer shift has been fit with the Debye model for a solid, and this fit yields a Mössbauer temperature, Θ_M, of 700(30) K. This Mössbauer temperature, Θ_M, of 700(30) K agrees rather well with the IR absorption observed for **1** at 518 cm^{-1} or 745 K, an absorption that is tentatively assigned to ν_{Fe-C} (see Supporting Information).

The temperature dependence of ΔE_Q has been fit with the Ingalls model[21] (see the inset to the left portion of Figure 4). This temperature dependence results from the removal of the 3-fold degeneracy of the t_{2g} orbitals by the low-symmetry component in the pseudooctahedral crystal field and the occupation by the five 3d electrons of the d_{xy} orbital and the approximately degenerate d_{xz} and d_{yz} orbitals with different energies. It is well-known[21] that these d_{xy}, d_{xz}, and d_{yz} orbitals yield different $\langle V_{zz}/e \rangle$ contributions of $+4/7\langle r^{-3}\rangle$, $-2/7\langle r^{-3}\rangle$, and $-2/7\langle r^{-3}\rangle$, respectively, to the electric-field gradient at the iron-57 nucleus. The fits yield splittings of the Fe(III) octahedral t_{2g} orbitals by the low-symmetry components of 355(4), 417(9), and 380(6) cm^{-1} for the Fe(1) and Fe(2) sites and their average, respectively. The difference in the former two values is fully consistent with the Fe−C bond distance and angle distortion values given in Table 2 and discussed above. Several $M_3[Fe(CN)_6]_2$ compounds, where M is Ni, Cd, Co, Cu, Mn, and Ca, and $K_3Fe(CN)_6$ exhibit[15b] a 0 K quadrupole splitting, which is either ca. 1 or 0.5 mm/s. This factor of 0.5 is explained[15b,c] by the difference in the t_{2g} orbital ordering. In the compounds with a ca. 1 mm/s 0 K quadrupole splitting, the t_{2g} orbital energy ordering is $d_{xy} < d_{xz} \sim d_{yz}$, whereas in the compounds with a ca. 0.5 mm/s 0 K quadrupole splitting, the t_{2g} orbital energy ordering is $d_{xz} \sim d_{yz} < d_{xy}$. Thus, in **1**, the ordering is $d_{xy} < d_{xz} \sim d_{yz}$, whereas in $K_3Fe(CN)_6$, it is $d_{xz} \sim d_{yz} < d_{xy}$.

Between 3 and 77 K, the Mössbauer spectra of **1** exhibit a broad virtually symmetric absorption that is highly characteristic of slow isotropic paramagnetic relaxation. Thus, the spectra have been fit with an isotropic relaxation model in the formalism of Dattagupta and Blume.[22] In these fits, the hyperfine field has been constrained to 30 T, a value that is consistent with the 3 K and 6.5 T applied field spectrum of the oxidized species[10] of the supramolecular complex $\{(DNP)_2[Fe(CN)_6]\}\cdot 20H_2O$ and **1** (see the Supporting Information). The value of the hyperfine field is related to the spin of the Fe cations. If the Fe cations are low-spin Fe(III) with $S = {}^1/_2$, a Fermi contact contribution[2e] of ca. 12.7 T is expected. The Fermi contact contribution will add to or subtract from the dipolar and orbital contributions to the hyperfine field to yield the effective hyperfine field. The value of 30 T is somewhat larger than the effective hyperfine field of 19.3(3) T reported[16b] for $KFe_3(CN)_6$ at 0.015 K. In these fits (see the right portion of Figure 3), the line width, Γ, has been constrained to 0.30 mm/s, a line width that is consistent with

DOI: 10.1021/acs.inorgchem.7b00540
Inorg. Chem. 2017, 56, 6477−6488

both that observed in the higher temperature spectra and that of the α-iron calibration spectra. Further, the quadrupole interaction, which is a small perturbation of the Zeeman magnetic interaction, has been constrained to be zero because of the symmetric nature of the observed spectral absorption. Thus, the fit of the 3−40 K relaxation spectra involved only three variables, the isomer shift, δ, the relaxation rate, ν, and the total spectral absorption area; their results are given in Table 3.

The temperature dependence of the isotropic relaxation rate, ν, observed for **1**, is shown in the inset to the right portion of Figure 4, and a natural ln−ln plot of the temperature dependence of the relaxation rate is shown in the right portion of Figure 4. Clearly, the temperature dependence of the relaxation rate may be divided into two parts. Between 3 and 20 K, on average ν = 94(2) MHz and is independent of the temperature, whereas, between 40 and 77 K, ν increases linearly with the temperature; the ν observed at 30 K seems to be intermediate.

It is well-known that spin−spin and spin−lattice coupling mechanisms control the rate of paramagnetic relaxation.[23] The former is temperature-independent and depends only on the distance between the spins on the Fe(III) ions of ca. 9.8 Å for the nearest contacts, in **1**. Hence, spin−spin relaxation is only effective at low temperature, i.e., between 3 and 20 K, temperatures at which the relaxation rate is essentially constant and equal to 94(2) MHz. Above 40 K, the relaxation rate is a linear function of the temperature, as is shown in the inset to the right portion of Figure 4, and this dependence is consistent with the linear fit line with a slope of 0.90(7), i.e., a slope of essentially 1, in the natural ln−ln plot of the relaxation rate versus temperature shown in the right portion of Figure 4. Above 40 K, the spin−lattice coupling relaxation mechanism dominates and the linear dependence of the relaxation rate with temperature indicates[23] that a one-phonon process is responsible for the spin−lattice relaxation. This interpretation of the temperature dependence of the relaxation rate is consistent with the presence of low-spin Fe(III) ions with $S = {}^1/_2$, and only $M_S = \pm{}^1/_2$ states, between which the relaxation takes place, are possible. Because there are no M_S excited states, the only possibility for observing a spin transition between these two states is through an interaction with phonons; i.e., the transition energy is taken from the energy of at least one phonon. Because a spin transition with $\Delta M_S = \pm 1$ does not require much energy, there is sufficient thermal energy available at 40 K, i.e., on average 28 cm^{-1}, and a one-phonon process explains the linear temperature dependence of the relaxation rate above 40 K.

In contrast, if the Fe cations have accessible excited-state M_S sublevels, the paramagnetic relaxation mechanism involves an activation over a barrier. This possibility is illustrated in the Arrhenius plot shown in the center panel of Figure 4. A fit of the inverse temperature dependence of ln ν between 40 and 77 K yields an activation energy of 48(6) K or 33(4) cm^{-1} for the relaxation process, with an attempt frequency of 400(40) MHz. The two parameters of this fit are highly negatively correlated, as is very often the case in Arrhenius plot fits. This possibility, which would involve, for instance, Fe(IV) cations with S = 1, is not retained because of its incompatibility with the low-temperature magnetic susceptibility measurements.

Rather unexpectedly, between 50 and 3 K, the average isomer shift of **1** increases substantially from −0.032 mm/s at 50 K to 0.13(1) mm/s at 3 K and departs significantly from the second-order Doppler shift observed between 50 and 295 K, a shift that predicts a 4.2 K extrapolated isomer shift of −0.032 mm/s, a value that is similar to that observed in the 3 K spectrum of **1** under an applied field of 5 T (see Figure 4, left). This increase in the isomer shift has been observed in spectra obtained on the same sample in two different spectrometers and cryostats and is difficult to explain. Usually, an increase in the isomer shift is associated with a decrease in the s-electron density at the iron-57 nucleus, a decrease that may result from an increase in the d-electron density or from an increase in the spin state. If the Fe cations in **1** are low-spin Fe(III) cations, as is indicated by all of the above Mössbauer spectral hyperfine parameters and the magnetic susceptibility measurements, the increase in the isomer shift cannot result from an increase in the d-electron density but could possibly result from an unexpected transition to high-spin Fe(III). This possibility has been dismissed because a low-spin-to-high-spin transition is virtually never observed with decreasing temperature in the low-temperature range of ca. 40 K.

Perhaps, as is clear from Figure 4, left and right, the apparent increase in the isomer shift and the onset of the slower relaxation process occur at approximately the same temperature of 40 K. Hence, it is possible that the increase in the isomer shift results from the change in the fitting model at 40 K. However, there is no clear basis for this effect in the isotropic relaxation model used, and a fit with a single broadened line gives the same isomer shift as the relaxation model does. In contrast, at 3 K in a 6.5 T applied field, the magnetic relaxation is not present, the fitting model is not a relaxation model, and the isomer shift agrees with the extrapolated value from the 50 to 295 K temperature dependence. The possibility that the increase in the isomer shift below 40 K is an artifact of the fitting procedure cannot be excluded but seems unlikely.

On the basis of the density functional theory (DFT) calculations of Nieuwpoort et al.[24] a difference in the s-electron density at the iron-57 nucleus of 1.191 electrons/$a_0{}^3$, where a_0 is the Bohr radius, is related to an increase in the isomer shift of 0.11 mm/s between $[Fe(CN)_6]^{3-}$ and $[Fe(CN)_6]^{4-}$. Hence, the herein observed increase in the isomer shift of 0.162 mm/s between the 4 K extrapolated value of −0.032 mm/s and the 3 K value of 0.13 mm/s corresponds to a very large decrease in the s-electron density of 1.73 electrons/$a_0{}^3$ or 11.68 electrons/Å^3, a value that seems unrealistic.

At this point, it is worth noting that the temperature dependence of the isomer shift in **1** between 50 and 295 K is virtually identical with that observed in $K_3Fe(CN)_6$ by Hazony[25] (see Figure S2). Unfortunately, Hazony did not report the uncertainties in the $K_3Fe(CN)_6$ isomer shifts, but the very small decrease in the isomer shift of ca. 0.015 mm/s in $K_3Fe(CN)_6$ compared to **1** is, no doubt, within the uncertainties of the reported isomer shifts. Indeed, the fit with the Debye model for a solid of the temperature dependence of the $K_3Fe(CN)_6$ isomer shifts (shown by the blue line in Figure S2) between 8 and 300 K yields a Mössbauer temperature, Θ_M, of 655(20) K, a value that is in reasonably good agreement with the 700(30) K value obtained for **1** between 50 and 295 K. Hence, it seems that between 50 and 295 K the isomer shift of the Mössbauer spectra confirms the presence of similar low-spin Fe(III) electronic environments in both $K_3Fe(CN)_6$ and **1**. The similarity in the lattice dynamics of both $K_3Fe(CN)_6$ and **1** is also supported by a comparison of the spectral f factors and spectral absorption areas in both compounds (see below and Figure S3).

At this point, it is of interest to try to explain why below ca. 50 K the isomer shift of **1** is substantially higher than expected both in comparison with its 50−295 K values and the values observed from 8 to 300 K in $K_3Fe(CN)_6$. Below ca. 50 K, it is quite likely that subtle structural changes may occur in the rather complex

DOI: 10.1021/acs.inorgchem.7b00540
Inorg. Chem. 2017, 56, 6477−6488

layered structure of **1**, changes that may change the low-symmetry splitting of the t_{2g} orbital energy difference between the d_{xy} ground-state orbital and the approximately degenerate d_{xz} and d_{yz} first excited-state orbitals from the average of 380 cm^{-1} observed above 50 K. If this energy splitting gradually decreases by say 100−200 cm^{-1} upon cooling from 50 to 3 K, there will be a Boltzmann increase in the electron population in the d_{xz} and d_{yz} first excited-state orbitals, an increase that will change the extent of π bonding between the low-spin Fe(III) nominally t_{2g} orbitals and the coordinated CN^- anions in the $[Fe(CN)_6]^{3-}$ moieties in **1**. Although perhaps modest, this change in the π bonding to the CN^- anions will influence the mixing of the molecular orbitals based on one or both of the $[Fe(CN)_6]^{3-}$ moieties in **1**, through the multitude of short contact distances with the molecular orbitals centered on the neighboring $(DPN)^{2+}$ cations. This mixing will consequently reduce the s-electron density at the iron nucleus of the low-spin Fe(III) ion and increase its isomer shift below 50 K. The spin−lattice coupling associated with the onset of slow paramagnetic relaxation below 50 K may also facilitate, to a significant extent, this molecular orbital mixing and decrease the s-electron density at the low-spin Fe(III) ion with a concomitant increase in its isomer shift. The importance of the onset of slow paramagnetic relaxation through reduced spin−lattice coupling is supported by the reversion of the isomer shift observed at 3 K in a 6.5 T applied field to a value consistent with that observed between 50 and 295 K (see the red point at 3 K in the left portion of Figure 4).

Finally, the temperature dependence of the logarithm of the Mössbauer spectral absorption area observed between 3 and 295 K has been fit with the Debye model for a solid (see the inset to the center portion of Figure 4); the resulting Debye temperature, Θ_D, is 137(2) K, a value that is substantially smaller than the Θ_M value of 700(30) K obtained from the isomer shifts. It is well-known[27] that the two temperatures, Θ_M and Θ_D, obtained from the two temperature dependencies are usually different because they depend on $\langle v^2 \rangle$ and $\langle x^2 \rangle$, respectively, where $\langle v^2 \rangle$ is the root-mean-square vibrational velocity of the iron-57 nuclide and $\langle x^2 \rangle$ is the root-mean-square displacement of the iron-57 nuclide. Unfortunately, there is no model-independent relationship[27] between these mean-square values, but the values of these temperatures reported[28] for other iron(III) complexes indicate that Θ_M, which is more sensitive to the high-frequency phonons, is often several times larger than Θ_D.

A comparison of the temperature dependence of the natural logarithm of the spectral area in **1**, reduced by 2.56, and of the recoil-free fraction[25] in $K_3Fe(CN)_6$ and their fits with the Debye model is shown in Figure S3. Because Θ_D in **1**, 137(2) K, is smaller than Θ_D in $K_3Fe(CN)_6$, 183(1) K, the lattice of **1** is softer than that of $K_3Fe(CN)_6$. It should be noted that Hazony[25] has used an Einstein model to fit the temperature dependence of the recoil-free fraction of $K_3Fe(CN)_6$, and thus no direct comparison between the reported[25] Einstein temperature and the Debye temperature reported herein is possible.

The paramagnetic relaxation mechanism is further investigated by the Mössbauer spectra measured between 3 and 295 K in an applied field varying between 3 and 6.5 T (see Figures S4 and S5 and Table S2). The fit of these spectra, as described in the Supporting Information, yields isomer shifts at 3, 77, 150, and 295 K, shown by the red circles in the left portion of Figure 4. At 77, 150, and 295 K, i.e., above 40 K, these isomer shifts obtained in an applied field agree completely with both those measured in zero applied field and the Debye model fit of the temperature dependence of the isomer shift shown by the solid line in this figure. Further, the 3 K applied field average isomer shift of −0.044 mm/s agrees very well with the extrapolated 4.2 K isomer shift of −0.032 mm/s. Hence, the applied field, as expected, slows down the paramagnetic relaxation to yield spectra with a partially resolved six-line Zeeman pattern, as shown in Figures S4 and S5.

In conclusion, the Mössbauer spectra of **1** are fully compatible with the presence of low-spin Fe(III) cations and show slow paramagnetic relaxation below 40 K and under zero applied magnetic field, a relaxation that is slowed down under an applied field of 6.5 T. The only observation that is difficult to explain is the concomitant increase in the isomer shift, under zero applied magnetic field, and the onset of slow paramagnetic relaxation below 40 K.

Photoluminescence Spectroscopy. The replacement of the chloride anions of the viologen, 1,1′-bis(2,4-dinitrophenyl)-4,4′-bipyridinium dichloride, $(DNP)Cl_2$, starting material with different $[M(CN)_6]^n$ anions resulted in a series of crystallographically and spectroscopically characterized compounds displaying different properties depending on the charge, *n*, and the nature of the metal, M, involved.[10,29] In **1**, exchanging the disordered chloride anions of $(DNP)Cl_2$ with $[Fe(CN)_6]^{3-}$ yields a structure in which the $[Fe(CN)_6]^{3-}$ anion is located close to the $(DNP)^{2+}$ organic electron acceptor because of the strong electrostatic interactions between the negatively charged cyanide terminal N atoms and the electron deficient 4,4′-bipyridinium core. These interactions between the $(DNP)^{2+}$ organic moieties and the $[Fe(CN)_6]^{3-}$ anions increase the spin−orbit coupling interactions at the Fe(III) ion, thus causing the nonluminescing $(DNP)^{2+}$ viologen to luminesce by the heavy-atom effect.[29] The type of radiative deactivation pathway and the energy of the emitted light depend, as expected, on the nature of the metal cation present.

Irradiating compound **1** with λ_{ex} = 300 nm radiation yields the broad structured fluorescence emission spectrum (see the right side of Figure 5), a spectrum that exhibits a vibronic progression with emission maxima at 412, 440, and 470 nm or 24270, 22730, and 21280 cm^{-1}, with differences of 1540 and 1450 cm^{-1}, respectively; the emission intensity increases with decreasing temperature between 90 and 25 K. The difference in the progression corresponds to aromatic ring C═C stretching normal modes with an energy in the range of 1450−1540 cm^{-1},

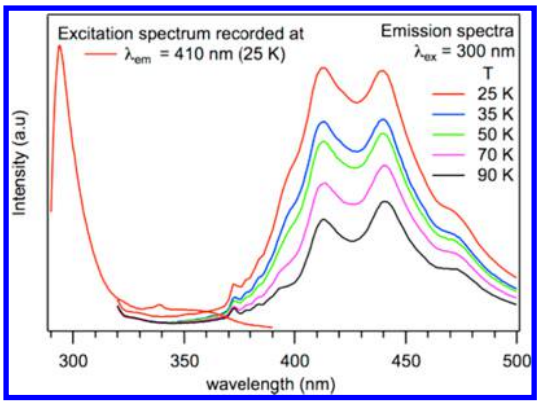

Figure 5. Right: Fluorescence emission spectra measured after excitation at λ_{ex} = 300 nm for **1** obtained at the indicated temperatures. Left: 25 K excitation absorption spectrum corresponding to λ_{em} = 410 nm, the wavelength of the maximum fluorescence found for **1**. The weak rather sharp signals at 340 and 375 nm in the excitation and fluorescence spectra, respectively, are due to Raman scattering and indicate that the fluorescence quantum efficiency is rather low.

DOI: 10.1021/acs.inorgchem.7b00540
Inorg. Chem. 2017, 56, 6477−6488

stretching modes that are observed at 1435 and 1481 cm^{-1} in the IR spectrum of **1** (see Figure S6). This observation indicates that the fluorescence is derived from the $(DNP)^{2+}$ viologen moiety.

The excitation absorption spectrum (see the left side of Figure 5), obtained while collecting λ_{em} = 410 nm fluorescence radiation, the wavelength of the maximum observed in the fluorescence emission spectrum, exhibits both an excitation absorption maximum at 294 nm, which may be attributed to an electric-dipole spin-allowed π-to-π^* transition in the $(DNP)^{2+}$ cation, and a much weaker band centered at ca. 360 nm. The weak fluorescence emission at 360 nm in **1** (see the right portion of Figure 5) overlaps with the excitation spectrum at this wavelength, indicating that the fluorescence emission arises from a weaker low-energy transition. With regard to this weak low-energy absorption transition, the Stokes shift is ca. 3500 cm^{-1}. Furthermore, the total luminescence intensity is quite low even at the lowest temperature, and the corresponding luminescence lifetime is shorter than the time resolution of less than 10 ns of the spectrophotometer.

In **1**, the excitation and fluorescence spectral profiles overlap and are, by comparison, very different from those observed for the recently published $(DNP)[Au(CN)_2]_2{\cdot}4H_2O$, gold(I) analogue,[29a] which exhibits an excitation absorption spectral profile between ca. 320 and 440 nm, a fluorescence emission spectral profile between ca. 520 and ca. 700 nm, and hence a profile gap of 80 nm. Further, **1** does not show any fluorescence emission upon excitation at λ_{ex} = 410 nm, the wavelength used in the study of the gold(I) analogue.[29a] This absence is consistent with the "lighter" paramagnetic Fe(III) ion in the $[Fe(CN)_6]^{3-}$ anion in comparison with the closed-shell, heavier Au(I) ion in the $(DNP)[Au(CN)_2]_2{\cdot}4H_2O$ analogue. In other words, the origin of the fluorescence in both **1** and the gold(I) compound is the same $(DNP)^{2+}$ moiety, a similar origin that is also supported by the similar shape of the fluorescence profiles of both compounds. However, the excitation absorption and fluorescence emission energies, and hence the nonradiative deactivation pathways, via internal conversion and intersystem crossing change depending on whether low-spin Fe(III) or Au(I) induces the emission.

Finally, we speculate that the most probable reason for the increase in the fluorescence is the large number of interionic and intermolecular contacts observed in the X-ray structure of **1** at 150(2) K between both the two $[Fe(CN)_6]^{3-}$ anions and the three $(DNP)^{2+}$ cations, all of which involve a contact distance of less than the sum of the two van der Waals radii involved in the contact. Of course, both the contact distances and the thermal parameters of the atoms and ions involved decrease to some extent upon cooling both between 150 and 90 K and between 90 and 25 K.

IR Spectral Results. IR spectroscopy has the advantage of providing useful information on the bond vibrational energies of certain bonds, such as the $C{\equiv}N^-$ and Fe−C bonds, on the much shorter time scale of molecular vibrations. The $C{\equiv}N^-$ stretching vibration, $\nu_{C{\equiv}N}$, in $[M(CN)_6]^n$ complexes, is known to be very sensitive to the oxidation and spin state of the M cation. The room temperature IR spectra of $(DNP)Cl_2$ and **1** are shown in Figure S6, and the corresponding IR absorption band assignments are given in Table S3.

The $\nu_{C{\equiv}N}$ absorption arising from the coordinated CN^- anions in **1** is observed at 2103 cm^{-1} and is shifted to lower energy by 14 cm^{-1} relative to the $\nu_{C{\equiv}N}$ band observed[30] at 2117 cm^{-1} in $K_3Fe(CN)_6$. Further, the Fe−C stretching vibration, ν_{Fe-C}, in **1** is tentatively observed at 518 cm^{-1} and is shifted by 3 cm^{-1} to lower energy relative to the analogous ν_{Fe-C} band observed[25,30] at 521 cm^{-1} in $K_3Fe(CN)_6$. It should be noted that $K_3Fe(CN)_6$ also exhibits an absorption band at 403 cm^{-1}, and it is possible that an analogous band appears just below 400 cm^{-1}, the low-energy limit of the IR spectrum of **1** shown in Figure S6. Because the Fourier transform IR spectra in Figure S6 have been obtained with a resolution of 4 cm^{-1}, only the shift of 14 cm^{-1} is significant and indicates the potential of a lower CN^- bond energy in **1** as a result of weak mixing of the molecular orbitals associated with the $[Fe(CN)_6]^{3-}$ anion with the $(DNP)^{2+}$ cations, a mixing that may become much more significant at lower temperatures.

EPR Spectrum. The 4 K X-band EPR measurement of a powder sample of **1** is shown in Figure S7. The 20 K EPR spectra of oriented single crystals of $K_3Fe(CN)_6$ diluted in $K_3Co(CN)_6$ have been studied in detail by Bleaney and co-workers[31] and then further discussed by Oosterhuis and Lang.[15a] Although there are some similarities between the spectra of powdered **1** and single crystals of $K_3Fe(CN)_6$ diluted in $K_3Co(CN)_6$, it is difficult to draw any conclusions from a comparison, in part because of the powder averaging in the spectra of **1**, which yields broad lines. A tentative comparison is given in the Supporting Information.

CONCLUSIONS

The electronic and magnetic properties of $K_3Fe(CN)_6$ have been extensively studied;[13−16] these studies have led to some controversial[18,25,26] and intensive investigations concerning the interpretation of its electronic[24] and spectroscopic[32] properties.

The presence of a formal electron transfer to the $(DNP)^{2+}$ cation from the Fe(III) ion in the $[Fe(CN)_6]^{3-}$ anions to yield an Fe(IV) ion in the $[Fe(CN)_6]^{2-}$ anions would be expected to lead to the intensively blue-to-violet-colored viologen radical cation. This color is not observed, and there is no experimental evidence either in the Mössbauer spectra or in the magnetic measurements to support the presence of Fe(IV) in **1**. Further, it is not surprising that, although Fe(II) ions are found[10] to participate in a formal electron transfer to $(DNP)^{2+}$ cations, the higher positive charge on the Fe(III) cations in the $[Fe(CN)_6]^{3-}$ anions in **1** makes a similar transfer of an electron to the $(DNP)^{2+}$ cations more difficult. The difficulty of this transfer in **1** is supported by the large difference in the ionization energy[33] of 1.41 eV, 16,363 K, or 11373 cm^{-1} between $[Fe(CN)_6]^{4-}$ and $[Fe(CN)_6]^{3-}$ in aqueous solution. Finally, the aqueous solution redox reactions of $[Fe(CN)_6]^{3-}$ with 1′-dimethyl-4,4′-bipyridinium dichloride or methyl viologen lead[34] to the reduction of Fe(III) cations to Fe(II) cations in $[Fe(CN)_6]^{4-}$. In conclusion, the experimental evidence rules out the presence of a formal electron transfer in **1**.

In contrast, the intense yellow color that appears immediately upon the reaction of $K_3Fe(CN)_6$ with $(DNP)Cl_2$ may well be indicative of a molecular orbital mixing through molecular orbital overlap between the $[Fe(CN)_6]^{3-}$ anions and the $(DNP)^{2+}$ cations to yield what are effectively supramolecular orbitals, as described for the first time by Kerr and Williams,[35] orbitals that provide the bonding between these anions and cations to produce the supramolecular bonding in **1**. Indeed, a similar yellow color was observed[36] upon the insertion of a *N*,*N*′-dibenzyl-4,4′-bipyridinium viologen cation inside a *p*-benzocrown ether as a result of molecular orbital interaction between the viologen cation and the crown ether. This molecular orbital mixing through molecular orbital overlap between the $[Fe(CN)_6]^{3-}$ anions and the $(DNP)^{2+}$ cations may correspond to a small drift of the electron density toward the $(DNP)^{2+}$ cation, as is indicated by the observed fluorescence that is induced by the

DOI: 10.1021/acs.inorgchem.7b00540
Inorg. Chem. 2017, 56, 6477−6488

$[Fe(CN)_6]^{3-}$ anions in **1**. The detailed nature of the molecular orbital mixing between the low-spin Fe(III) ions in the $[Fe(CN)_6]^{3-}$ anions and the $(DNP)^{2+}$ cation acceptors in **1** remains unknown, and DFT calculations have, to date, failed to provide details of the molecular orbital bonding because of the extended supramolecular nature of **1**.

Thus, our search for a formal electron transfer from the $[Fe(CN)_6]^{3-}$ anions to the $(DNP)^{2+}$ cation acceptors in **1** has been unsuccessful, as determined by the techniques used herein. Rather, these experimental measurements indicate a significant molecular orbital mixing between the anions and cations, a mixing that leads to both the unexpectedly high Mössbauer spectral isomer shifts observed below 50 K and the magnetic properties observed for **1**. This molecular orbital mixing, in conjunction with spin−orbit coupling, also leads to the fluorescence observed from the viologen dication in **1**.

■ ASSOCIATED CONTENT

Supporting Information

The Supporting Information is available free of charge on the ACS Publications website at DOI: 10.1021/acs.inorgchem.7b00540.

Comparisons of magnetic and Mössbauer spectral results on **1** and $K_3[Fe(CN)_6]$, Mössbauer spectra of **1** obtained in applied magnetic fields at different temperatures, Mössbauer spectral parameters for **1** between 50 and 295 K, and IR and EPR spectral results (PDF)

Accession Codes

CCDC 1476568 contains the supplementary crystallographic data for this paper. These data can be obtained free of charge via www.ccdc.cam.ac.uk/data_request/cif, or by emailing data_request@ccdc.cam.ac.uk, or by contacting The Cambridge Crystallographic Data Centre, 12, Union Road, Cambridge CB2 1EZ, UK; fax: +44 1223 336033.

■ AUTHOR INFORMATION

Corresponding Authors

*E-mail: ahmed.soliman.abouelwafa@volkswagen.de.
*E-mail: glong@mst.edu.
*E-mail: annie.powell@kit.edu.

ORCID

Gary J. Long: 0000-0002-6573-5927
Annie K. Powell: 0000-0003-3944-7427

Present Address

¶A.S.A.: Department of Batteries and Energy Carrier Research, Volkswagen AG, Berliner Ring 2, D-38440 Wolfsburg, Germany.

Notes

The authors declare no competing financial interest.

■ ACKNOWLEDGMENTS

This work was supported by the DFG, Center for Functional Nanostructures, and the Swiss National Science Foundation (Contract 200020-125175). We acknowledge the Synchrotron Light Source ANKA for a provision of instruments at the SCD beamline. The work of F.G. was supported by the Fonds National de la Recherche Scientifique, Belgium, through Grants 9.456595 and 1.5.064.05.

■ REFERENCES

(1) (a) Bogani, L.; Wernsdorfer, W. Molecular Spintronics Using Single-molecule Magnets. *Nat. Mater.* **2008**, *7*, 179−186. (b) Mannini, M.; Pineider, F.; Sainctavit, P.; Danieli, C.; Otero, E.; Sciancalepore, C.; Talarico, A. M.; Arrio, M. A.; Cornia, A.; Gatteschi, D.; Sessoli, R. Magnetic Memory of a Single-molecule Quantum Magnet Wired to a Gold Surface. *Nat. Mater.* **2009**, *8*, 194−197.

(2) (a) Sessoli, R.; Tsai, H. L.; Schake, A. R.; Wang, S.; Vincent, J. B.; Folting, K.; Gatteschi, D.; Christou, G.; Hendrickson, D. N. High-spin Molecules: $[Mn_{12}O_{12}(O_2CR)_{16}(H_2O)_4]$. *J. Am. Chem. Soc.* **1993**, *115*, 1804−1816. (b) Sessoli, R.; Gatteschi, D.; Caneschi, A.; Novak, M. A. Magnetic Bistability in a Metal-ion Cluster. *Nature* **1993**, *365*, 141−143. (c) Ako, A. M.; Hewitt, I. J.; Mereacre, V.; Clérac, R.; Wernsdorfer, W.; Anson, C. E.; Powell, A. K. A Ferromagnetically Coupled Mn19 Aggregate with a Record $S = 83/2$ Ground Spin State. *Angew. Chem., Int. Ed.* **2006**, *45*, 4926−4929. (d) Zadrozny, J. M.; Xiao, D. J.; Atanasov, M.; Long, G. J.; Grandjean, F.; Neese, F.; Long, J. R. Magnetic Blocking in a Linear Iron(I) Complex. *Nat. Chem.* **2013**, *5*, 577−581. (e) Zadrozny, J. M.; Xiao, D. J.; Long, J. R.; Atanasov, M.; Neese, F.; Grandjean, F.; Long, G. J. Mössbauer Spectroscopy as a Probe of Magnetization Dynamics in the Linear Iron(I) and Iron(II) Complexes $[Fe(C(SiMe_3)_3)_2]^{1-/0}$. *Inorg. Chem.* **2013**, *52*, 13123−13131.

(3) (a) Iijima, S.; Mizutani, F.; Mitsumi, M.; Matsumoto, N.; Ōkawa, H. Slow Paramagnetic Relaxation and Magnetic Splittings in Mössbauer Spectra Observed for Mixed-metal Assemblies $\{NBu_4MFe(ox)_3\}_x$ (NBu_4^+ = tetra(n-butyl) ammonium ion; ox2 = oxalate ion; M = Zn^{2+}, Ni^{2+}, Mn^{2+}). *Inorg. Chim. Acta* **1996**, *253*, 47−51.

(4) (a) Wignall, J. W. G. Mössbauer Line Broadening in Trivalent Iron Compounds. *J. Chem. Phys.* **1966**, *44*, 2462−2467. (b) Wickman, H. H.; Klein, M. P.; Shirley, D. A. Paramagnetic Hyperfine Structure and Relaxation Effects in Mössbauer Spectra: Fe^{57} in Ferrichrome *A*. *Phys. Rev.* **1966**, *152*, 345−357. (c) Wickman, H. H.; Wertheim, G. K. Mössbauer Hyperfine Spectra of Fe^{3+} in Corundum: Magnetic-and Crystal-Field Effects. *Phys. Rev.* **1966**, *148*, 211−217.

(5) (a) Witten, E. H.; Reiff, W. M.; Lázár, K.; Sullivan, B. W.; Foxman, B. M. The Ferric Chloride-.alpha.-diamine System. 3. X-ray Crystallographic, Magnetic Susceptibility, and Zero- and High-field Mössbauer Spectroscopy Investigation of Bis(2,2′-bipyridine)dichloroiron(2+) Tetrachloroferrate(2-): Slow Paramagnetic Relaxation and Magnetic Ordering of Complex Bimetallic Salts. *Inorg. Chem.* **1985**, *24*, 4585−4591. (b) Reiff, W. M.; Witten, E. H. The Ferric Chloride α-DI-imine SystemVI: Electronic Structure of the Dimethyl Formamide Addcut of Mono-1,10-phenanthroline Ferric Chloride and the By-product, tris-1,10-phenanthroline Ferrous μ-oxo-bis[trichloro ferrate(III)]; Field Induced Slow Paramagnetic Relaxation in Monomeric Ferric Complexes. *Polyhedron* **1984**, *3*, 443−449.

(6) (a) Veidis, M. V.; Witten, E. H.; Reiff, W. M.; Brennan, T. F.; Garafalo, A. R. The Ferric Chloride α-Di-imine System. Part II. X-ray Structure Determination of 2,9-Di-CH_3phenathrolinium Tetrachlorferrate(III). *Inorg. Chim. Acta* **1981**, *54*, L133−L135. (b) Edwards, P. R.; Johnson, C. E. Mössbauer Hyperfine Interactions in Tetrahedral Fe(III) Ions. *J. Chem. Phys.* **1968**, *49*, 211−216.

(7) (a) Hall, G. R.; Hendrickson, D. N. Ferric Tris(dithiocarbamate) Spin Equilibrium Revisited. Variable-temperature (4.2−296.deg.K) Magnetic Susceptibility, (30−300.deg.K) Infrared, and (4.2−85.deg.K) Electron Paramagnetic Resonance Data. *Inorg. Chem.* **1976**, *15*, 607−618. (b) Merrithew, P. B.; Rasmussen, P. G. Temperature Dependence of the Mössbauer Spectra of Several Iron(III) Dithio chelates. *Inorg. Chem.* **1972**, *11*, 325. (c) Rickards, R.; Johnson, C. E.; Hill, H. A. O. Mössbauer-Effect Study of Some Iron(III) *N,N*-Dialkyldithiocarbamates. *J. Chem. Phys.* **1968**, *48*, 5231−5238. (d) Ewald, A. H.; Martin, R. L.; Sinn, E.; White, A. H. Electronic Equilibrium between the $^6A_1$ and $^2T_2$ States in Iron(III) Dithio-chelates. *Inorg. Chem.* **1969**, *8*, 1837−1846. (e) Fiddy, J. M.; Hall, I.; Grandjean, F.; Long, G. J.; Russo, U. Temperature Dependence of the Mössbauer Spectra of Several Iron(III) Trisdithiocarbamate Complexes. *J. Phys.: Condens. Matter* **1990**, *2*, 10091−10108.

(8) (a) Cambi, L.; Szego, L. Über die Magnetische Susceptibilität der Komplexen Verbindungen. *Ber. Dtsch. Chem. Ges. B* **1931**, *64*, 2591−2598. (b) Cambi, L.; Szego, L. Über die magnetische Susceptibilität der komplexen Verbindungen (II. Mitteil.). *Ber. Dtsch. Chem. Ges. B* **1933**, *66*, 656−661.

DOI: 10.1021/acs.inorgchem.7b00540
Inorg. Chem. 2017, 56, 6477−6488

(9) (a) Frank, E.; Abeledo, C. R. Mössbauer Effect in Iron(III) Dithiocarbamates. *Inorg. Chem.* **1966**, *5*, 1453−1461. (b) Golding, R. M.; Whitfield, H. J. Mössbauer Study of Several Iron (III) Dithiocarbamates. *Trans. Faraday Soc.* **1966**, *62*, 1713−1716.
(10) Abouelwafa, A. S.; Mereacre, V.; Balaban, T. S.; Anson, C. E.; Powell, A. K. Photo- and Thermally-enhanced Charge Separation in Supramolecular Viologen−hexacyanoferrate Complexes. *CrystEngComm* **2010**, *12*, 94−99.
(11) (a) Sheldrick, G. M. *SADABS (the Siemens Area Detector Absorption Correction)*; University of Göttingen: Göttingen, Germany, 2005. (b) Sheldrick, G. M. Crystal Structure Refinement with *SHELXL*. *Acta Crystallogr.* **2015**, *C71*, 3−8.
(12) Bain, G. A.; Berry, J. F. Diamagnetic Corrections and Pascal's Constants. *J. Chem. Educ.* **2008**, *85*, 532−536.
(13) (a) Katila, T.; Leskelä, M.; Niinistö, L.; Riski, K. J.; Valkonen, J.; Ylä-Jääski, J. Y. Crystal Structure and Mössbauer Measurements of Monoclinic Sodium Hexacyanoferrate(III) Dihydrate. *J. Solid State Chem.* **1980**, *35*, 341−346. (b) Morioka, Y.; Toriumi, K.; Ito, T.; Saito, A.; Nakagawa, I. Crystal Structures of the Room- and Low-Temperature Phases of Monoclinic Potassium Ferricyanide. *J. Phys. Soc. Jpn.* **1985**, *54*, 2184−2189. (c) Note that in part b an apparently wrong space group designation, $P2_1/n$, was used at 100 K. The correct designation appears to be $P2_1/m$..
(14) (a) McKim, F. R.; Wolf, W. P. The Susceptibility and Magnetic Specific Heat of Potassium Ferricyanide at Low Temperatures. *Proc. Phys. Soc., London, Sect. B* **1956**, *69*, 1231−1236. (b) Baker, J.; Figgis, B. N. Magnetic Properties of Some Low-spin Iron(III) Compounds. *J. Chem. Soc., Dalton Trans.* **1975**, 598−602. (c) Figgis, B. N.; Martin, D. J. J. The Magnetic Susceptibilities of Some Trinuclear Copper(II) Compounds. *J. Chem. Soc., Dalton Trans.* **1972**, 2174−2176.
(15) (a) Oosterhuis, W. T.; Lang, G. Mössbauer Effect in $K_3Fe(CN)_6$. *Phys. Rev.* **1969**, *178*, 439−456. (b) Hrynkiewicz, A. Z.; Sawicka, B.; Sawicki, J. Temperature Dependence of the Electric Field Gradient in Ferricyanides. *Proceedings of the Conference on Applications of the Mössbauer Effect*, Tihany, Hungary, June 17−21, 1969; Dezsi, I., Ed.; Akademiai Kiado: Budapest, Hungary, 1971; p 731−737. (c) Hazony, Y. $3d(t_{2g})$ Density Distribution in Covalent Transition Metal Complexes from Mössbauer and EPR Experiments. *J. Phys. C: Solid State Phys.* **1972**, *5*, 2267−2275.
(16) (a) Shinohara, M.; Ishigaki, A.; Ôno, K. Improved Demagnetization Cryostat for Mössbauer Effect Experiments. *Jpn. J. Appl. Phys.* **1968**, *7*, 170−173. (b) Ôno, K.; Shinohara, M.; Ito, A.; Sakai, N.; Suenaga, M. Observation of Zero-Point Spin Deviation in Antiferromagnetic $K_3Fe(CN)_6$. *Phys. Rev. Lett.* **1970**, *24*, 770−771.
(17) (a) Samain, L.; Grandjean, F.; Long, G. J.; Martinetto, P.; Bordet, P.; Strivay, D. Relationship between the Synthesis of Prussian Blue Pigments, Their Color, Physical Properties, and Their Behavior in Paint Layers. *J. Phys. Chem. C* **2013**, *117*, 9693−9712. (b) Grandjean, F.; Samain, L.; Long, G. J. Characterization and Utilization of Prussian Blue and its Pigments. *Dalton Trans.* **2016**, *45*, 18018−18044.
(18) (a) Oosterhuis, W. T.; Lang, G.; Debenedetti, S. Mössbauer Spectra of $K_3Fe(CN)_6$ at Low Temperatures. *Phys. Lett. A* **1967**, *24*, 346−347. (b) Oosterhuis, W. T.; Debenedetti, S.; Lang, G. Magnetic Hyperfine Structure in the Mössbauer Spectra of $K_3Fe(CN)_6$. *Phys. Lett. A* **1968**, *26*, 214−216. (c) Golding, R. M. A Theoretical Investigation of the Temperature Dependence of the Quadrupole Splitting of Low Spin Ferric Compounds. *Mol. Phys.* **1967**, *12*, 13−23. (d) Johansson, L. Y.; Larsson, R.; Blomquist, J.; Cederstrom, C.; Grapengiesser, S.; Helgeson, U.; Moberg, L. C.; Sundbom, M. X-ray Photoelectron and Mössbauer Spectroscopy on a Variety of Iron Compounds. *Chem. Phys. Lett.* **1974**, *24*, 508−513. (e) Hikita, T.; Itoh, K. ^{57}Fe Mössbauer Spectroscopy of Potassium Ferricyanide $[K_3Fe(CN)_6]$. *J. Kor. Phys. Soc.* **1998**, *32*, S679−S681.
(19) Gütlich, P.; Bill, E.; Trautwein, A. X. *Mössbauer Spectroscopy and Transition Metal Chemistry, Fundamentals and Applications*; Springer: Berlin, 2011; p 85.
(20) Abbas, G.; Lan, Y.; Mereacre, V.; Wernsdorfer, W.; Clérac, R.; Buth, G.; Sougrati, M. T.; Grandjean, F.; Long, G. J.; Anson, C. E.; Powell, A. K. Magnetic and ^{57}Fe Mössbauer Study of the Single Molecule Magnet Behavior of a Dy_3Fe_7 Coordination Cluster. *Inorg. Chem.* **2009**, *48*, 9345−9355.
(21) Ingalls, R. Electric Field Gradient Tensor in Ferrous Compounds. *Phys. Rev. A* **1964**, *133*, 787−795.
(22) Dattagupta, S.; Blume, M. Stochastic Theory of Line Shape. I. Nonsecular Effects in the Strong-collision Model. *Phys. Rev. B* **1974**, *10*, 4540−4550.
(23) Mørup, S. In *The Time Domain in Surface and Structural Dynamics*; Long, G. J., Grandjean, F., Eds.; Kluwer: Dordrecht, The Netherlands, 1988; pp 309−333.
(24) Nieuwpoort, W. C.; Post, D.; van Duijnen, P. Th. Calibration Constant for ^{57}Fe Mössbauer Isomer Shifts Derived from Ab-initio Self-consistent-field Calculations on Octahedral FeF_6 and $Fe(CN)_6$ clusters. *Phys. Rev. B: Condens. Matter Mater. Phys.* **1978**, *17*, 91−98.
(25) Hazony, Y. Mössbauer Investigation of the Intra- and Inter-Molecular Dynamics of $K_3Fe(CN)_6$ − Electron-Phonon Instability at ∼ 130 K. *Discuss. Faraday Soc.* **1969**, *48*, 148−155.
(26) Lang, G.; Dale, B. W. Comment on Recent Misinterpretations of the Mössbauer and ESR Spectra of Low-spin Fe III Complexes. *J. Phys. C: Solid State Phys.* **1973**, *6*, L80−L82.
(27) Shenoy, G. K.; Wagner, F. E.; Kalvius, G. M. *Mössbauer Isomer Shifts*; North-Holland: Amsterdam, The Netherlands, 1978; p 49.
(28) (a) Owen, T.; Grandjean, F.; Long, G. J.; Domasevitch, K. V.; Gerasimchuk, N. Synthesis and Characterization of Two Intensely Colored Tris(benzoylcyanoxime)iron(II) Anionic Complexes. *Inorg. Chem.* **2008**, *47*, 8704−8713. (b) Möchel, A.; Sergueev, I.; Nguyen, N.; Long, G. J.; Grandjean, F.; Johnson, D. C.; Hermann, R. P. Lattice Dynamics in the $FeSb_3$ Skutterudite. *Phys. Rev. B: Condens. Matter Mater. Phys.* **2011**, *84*, 064302−9.
(29) (a) Abouelwafa, A. S.; Anson, C. E.; Hauser, A.; Patterson, H. H.; Baril-Robert, F.; Li, X.; Powell, A. K. Photophysical Properties of $\{[Au(CN)_2]^-\}_2$ Dimers Trapped in a Supramolecular Electron-Acceptor Organic Framework. *Inorg. Chem.* **2012**, *51*, 1294−1301. (b) Koziar, J. C.; Cowan, D. O. Photochemical Heavy-atom Effects. *Acc. Chem. Res.* **1978**, *11*, 334−341.
(30) Nyquist, R. A.; Kagel, R. O. *Handbook of Infrared and Raman Spectra of Inorganic Compounds and Organic Salts*; Elsevier: New York, 1971.
(31) (a) Baker, J. M.; Bleaney, B.; Bowers, K. D. Paramagnetic Resonance in Some Complex Cyanides of the Iron Group I: Experimental Results. *Proc. Phys. Soc., London, Sect. B* **1956**, *69*, 1205−1215. (b) Bleaney, B.; O'Brien, M. C. M. Paramagnetic Resonance in Some Complex Cyanides of the Iron Group II. Theory. *Proc. Phys. Soc., London, Sect. B* **1956**, *69*, 1216−1230.
(32) Gray, H. B.; Beach, N. A. The Electronic Structures of Octahedral Metal Complexes. I. Metal Hexacarbonyls and Hexacyanides. *J. Am. Chem. Soc.* **1963**, *85*, 2922−2927. (b) Alexander, J. J.; Gray, H. B. Electronic Structures of Hexacyanometalate Complexes. *J. Am. Chem. Soc.* **1968**, *90*, 4260−4271.
(33) Seidel, R.; Thürmer, S.; Moens, J.; Geerlings, P.; Blumberger, J.; Winter, B. Valence Photoemission Spectra of Aqueous $Fe^{2+/3+}$ and $[Fe(CN)_6]^{4-/3-}$ and Their Interpretation by DFT Calculations. *J. Phys. Chem. B* **2011**, *115*, 11671−11677.
(34) Dharmarathne, L.; Ashokkumar, M.; Grieser, F. Reaction of Ferricyanide and Methyl Viologen with Free Radicals Produced by Ultrasound in Aqueous Solutions. *J. Phys. Chem. A* **2012**, *116*, 7775−7782.
(35) Williams, F.; Kerr, C. M. L. Supramolecular Bonding Orbitals from Molecular Antibonding Orbitals. Structure of the Radical Anion of Sulfuryl Chloride. *J. Am. Chem. Soc.* **1971**, *93*, 2805−2807.
(36) Kuwabara, T.; Sugiyama, M.; Nanasawa, M. Photochromism of Viologens Included in Crown Ether Cavity. *Photochem. Photobiol.* **2001**, *73*, 469−472.

DOI: 10.1021/acs.inorgchem.7b00540
Inorg. Chem. 2017, 56, 6477−6488